## LANGMUIR

pubs.acs.org/Langmuir Article

# Engineering the Structure and Rheological Properties of P407 Hydrogels via Reverse Poloxamer Addition

Joanna M. White, Ally Garza, James J. Griebler, Frank S. Bates, and Michelle A. Calabrese\*



Cite This: Langmuir 2023, 39, 5084-5094



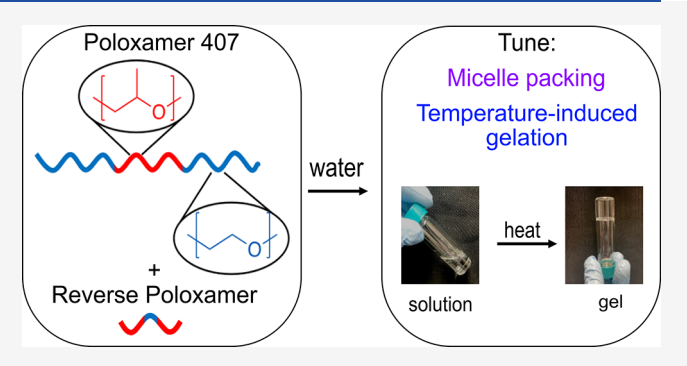
**ACCESS** 

III Metrics & More

Article Recommendations

Supporting Information

ABSTRACT: Aqueous solutions of poloxamer 407 (P407), a commercially available and nontoxic ABA triblock polymer (PEO-PPO-PEO), undergo a solution-to-gel transition with increasing temperature and are promising candidates for injectable therapeutics. The gel transition temperature, modulus, and structure are all dictated by polymer concentration, preventing independent tuning of these properties. Here, we show that addition of BAB reverse poloxamers (RPs) to P407-based solutions dramatically alters the gelation temperature, modulus, and morphology. Gelation temperature and RP localization within the hydrogel are dictated by RP solubility. Highly soluble RPs increase gelation temperature and incorporate primarily into the micelle



corona regions. Alternatively, RPs with low aqueous solubility decrease gelation temperature and associate within the micelle core and core—corona interface. These differences in RP localization have significant implications for the hydrogel modulus and microstructure. The ability to tune gelation temperature, modulus, and structure through RP addition allows for the design of thermoresponsive materials with specific properties that are unobtainable with neat P407-based hydrogels.

#### **■ INTRODUCTION**

Thermoresponsive polymeric materials that behave as liquids at low temperatures and form physical gels upon heating have broad applications in drug delivery and biological engineering. 1-3 For example, thermoresponsive aqueous formulations composed of polymers loaded with cells and growth factors have been examined as potential scaffolds for wound and tissue repair.<sup>4,5</sup> For such healing applications, the formulation ideally behaves as a low-viscosity fluid at room temperature to allow for noninvasive injection, but gels with increasing temperature, giving the formulation the mechanical strength to support damaged tissue and a high water content to promote diffusion of nutrients during repair.<sup>4,5</sup> Similarly, therapeutics have been incorporated into thermoresponsive polymer solutions to yield syringeable medications that can adhere to biological barriers, allowing for transocular, 6-8 transtympanic, 9-12 and transdermal 13,14 delivery. In certain delivery systems, such as those used for stem cell therapy, the formulations must remain a low-viscosity liquid during injection, as higher injection forces required by gels would damage the cells. 15 Further, precise tuning of the gel's mechanical properties is also necessary, as small variations in the modulus can drastically affect cell differentiation. 15,16 Unfortunately, engineering such thermoresponsive materials is difficult because each application requires unique gel properties, e.g., gelation temperature, modulus, and gelation time following administration.

In addition to favorable temperature-dependent rheological transitions, certain applications, such as drug delivery and

protein immobilization, require direct design of macromolecular structure.<sup>17–19</sup> For example, molecular crowding and confinement of proteins in micelle-forming polymer gels can reduce aggregation and denaturation, enhancing the thermal stability of protein-based therapeutics.<sup>18–22</sup> A high chain density within the coronal region of the micelle is desired to maximize this crowding effect. By contrast, in drug delivery, minimizing the coronal chain density aids in diffusion of drugs out of micelles.<sup>17</sup> Overall, the ability to tune corona chain density, gelation temperature, and gel modulus independently of one another is crucial for engineering formulations for targeted applications.

A widely studied class of thermoresponsive hydrogels are aqueous solutions of poloxamers, ABA triblock polymers consisting of poly(ethylene oxide) (PEO) end blocks (A), and a poly(propylene oxide) (PPO) midblock (B). These polymers have low toxicity and are commercially available in a range of molecular compositions, resulting in FDA approval of poloxamer-containing products for a wide variety of applications.<sup>23–33</sup> One such poloxamer, P407, has attracted

Received: January 9, 2023 Revised: March 14, 2023 Published: March 27, 2023





Table 1. Molecular Characterization Data for P407 and Relevant Reverse Poloxamers

Polymer	$M_{\rm n}~[{ m kDa}]^a$	$x_{\text{PEO}}^{b}$	$M_{\rm n,PPO}~[{ m kDa}]^c$	$Structure^d$
P407	11.7	0.72	3.4	<b>~~~~</b>
10R5	2.1	0.52	1.0	<b>✓</b>
17R2	2.3	0.26	1.7	<b>✓</b>
17R4	3.0	0.42	1.7	<b>✓</b>
25R2	3.5	0.25	2.6	<b>~</b>

<sup>&</sup>quot;Number-average molecular weight, characterized via SEC-MALS. <sup>b</sup>PEO block mass fraction, characterized via <sup>1</sup>H NMR. <sup>c</sup>Number-average molecular weight of the PPO block, characterized by SEC-MALS and <sup>1</sup>H NMR. <sup>d</sup>PEO: blue structure; PPO: red structure.

particular attention for clinical applications due to its lower critical solution temperature (LCST) behavior which drives micellization and gelation behavior with increasing temperature in aqueous solutions of the 15–30% (w/v) polymer. 12,34–39 At refrigeration temperatures (4 °C), P407 chains exist as unimers in solution, as the solubility of both blocks in water is sufficiently high. With increasing temperature, the interactions between water and PPO become less favorable and the PPO midblock dehydrates, causing chains to assemble into spherical micelles with PPO cores and PEO coronas. Near body temperature (37 °C), interactions between neighboring micelle corona blocks drive the assembly of P407 micelles into cubic packings, causing the formation of a physical hydrogel. 44–47

Unfortunately, the ability to tune the lattice packing (face-centered cubic vs body-centered cubic), gelation temperature, and gel modulus of neat aqueous P407 solutions independently is not possible. Increasing the P407 concentration increases the maximum storage modulus of the gel,  $G'_{\text{max}}$ , when measured at a constant frequency with increasing temperature, but simultaneously decreases the temperature at the onset of gelation,  $T_{\text{onset}}$ . This relationship limits the clinical applicability of neat P407 solutions, as formulations with a clinically useful modulus often have a  $T_{\text{onset}}$  below room temperature. Additionally, therapeutic small-molecule additives typically decrease  $T_{\text{onset}}$  and  $G'_{\text{max}}$ , further hampering formulation design.  $S_{\text{p,28,32,47}}$ 

Previously, certain reverse poloxamers (RPs), BAB triblock polymers composed of the same chemistries as poloxamers but arranged in the reverse order, have been added to P407 solutions to alter the gelation behavior.<sup>47,49-51</sup> While ABA poloxamers form micelles over a wide range of block fractions, micellization of RPs results in a significant decrease in chain conformational entropy, as the chains must form loops in order for both PPO blocks to insert into the same core. 50,52-54 As a result, a high PEO molecular weight is required for RPs to form micelles in water. 53,55 While this formulation space is underexplored, the limited work on solutions of P407 with RPs shows that varying RP concentration, identity, and composition alters the gelation temperature and modulus of P407. Xie et al. so measured the rheology of 20% (w/w) solutions of P407 with 17R4, a low-molecular-weight RP with 40% PEO. The authors showed that 17R4 addition broadens the gel transition compared to neat P407 solutions, resulting in the development of a soft gel  $(G' = 10^1 - 10^2 \text{ Pa})$  prior to a hard gel  $(G' = 10^3 -$ 10<sup>4</sup> Pa) formation at elevated temperatures. The authors hypothesized that the low-molecular-weight 17R4 chains remain in solution above the P407 micellization temperature, sterically screening the interactions among P407 micelles and hindering assembly and hard gel formation.<sup>50</sup> Unfortunately,

characterization of the underlying microstructure within the soft and hard gel regimes is lacking.

A similar increase in the gelation temperature has been observed upon addition of 25R4, 47,49,56 a higher-molecularweight RP with the same PEO fraction (40%) as 17R4. Our recent work utilizing rheology, small-angle X-ray scattering (SAXS), and differential scanning calorimetry (DSC) suggests that this increase in gelation temperature stems from a twostep dehydration mechanism that occurs upon 25R4 addition. Consistent with prior reports, 49,56 in the first step, P407 micelles are formed while 25R4 chains remain in solution. As proposed by Xie et al.,50 these low-molecular-weight 25R4 chains hinder interactions among neighboring P407 micelles and thus prevent gelation. In the second step, as temperature is increased further, the PPO blocks in 25R4 dehydrate to form multichain bridges across P407 micelles. 47,49 These bridges serve as additional physical cross-links, leading to an increase in the maximum storage modulus  $(G'_{max})$  upon 25R4 addition. 47,49,57 This rheological enhancement remains in drug-loaded formulations, providing a mechanism for improving the stability of gels that suffer from low gelation moduli with drug addition. 47,51 While neat RPs with lower PEO fractions do not form micelles in water, the addition of 31R1, an RP with 10% PEO, to P407 solutions also enhances  $G'_{\text{max}}$ but reduces  $T_{\text{onset}}$ . 47 Unlike in the P407/25R4 system, rheology, DSC, and SAXS showed that incorporation of 31R1 drives the formation of 31R1/P407 mixed micelles.

Our previous work on 25R4 and 31R1 showed that RP addition can be a route for independently tuning  $T_{\rm onset}$  and  $G'_{\rm max}$ , with the RP identity influencing whether  $T_{\rm onset}$  increased or decreased with RP addition. Thus, a strong understanding of RP incorporation into P407 solutions can enable the intentional design of macromolecular structure and external properties of P407 hydrogels via RP addition. While there are limited isolated reports of altering P407 gelation via addition of other commercially available RPs, a comprehensive study of the structure—property relationships as a function of RP concentration and identity is lacking. The absence of such detailed structural information about the incorporation mechanisms makes predicting rheological and structural properties a priori difficult, limiting systematic design of materials for desired applications.

Here rheology, SAXS, and DSC are used to elucidate the mechanism of incorporation of four different RPs into P407-based hydrogels. By evaluating several concentrations of RPs that have a variety of PPO block molecular weights ( $M_{\rm n,PPO}$ ) and block mass fractions of PPO ( $x_{\rm PPO}$ ), we identify amphiphile parameters that govern the mechanisms of RP incorporation and gelation in mixed RP/P407 systems. Using this comprehensive fundamental understanding, we develop

general design guidelines for engineering thermoresponsive materials with specific gelation temperatures, gel moduli, and morphology for desired applications in medicine and beyond.

#### MATERIALS AND METHODS

Poloxamers and Reverse Poloxamers. All polymers used in this study are commercially available and were used as received without further purification. Kolliphor P407 and 10R5 were obtained from Sigma-Aldrich, 17R2 and 17R4 from Stepan, and 25R2 from BASF. Commercially, each RP is named XXRZ, where XX refers to the approximate number-average molecular weight of the PPO block  $(M_{n,PPO})$  divided by 100 and Z is the approximate mass fraction of the PEO block  $(x_{PEO})$  divided by 10 (Table 1). The total molecular weight and mass fraction of each block were confirmed using sizeexclusion chromatography (SEC) with differential refractive index and light scattering detection and <sup>1</sup>H NMR, respectively, which vary slightly from the target values associated with the naming convention (Figures S1 and S2). All solutions were prepared containing 15% (w/ v) P407 with the addition of a set molar ratio of P407:RP. Polymers were dissolved in HPLC-grade water and stirred at refrigerator temperature (4 °C) for at least 24 h prior to measurement.

Temperature-Dependent Oscillatory Rheology. To probe the rheological properties over the course of gelation, temperature ramps were performed under small-amplitude oscillatory shear on an Anton Paar MCR 302 rheometer using a 26.7 mm diameter double-gap geometry. The samples were heated at a rate of 1 °C/min with  $\omega = 1$ rad/s and  $\gamma = 1\%$ , and the storage (G') and loss (G") moduli were measured as a function of temperature. While neat P407 solutions display a single, sharp increase in both G' and G'' with increasing temperature, addition of RPs can alter the shape of this transition. Certain formulations displayed a transition from a liquid to "soft gel" (G' = 10-1000 Pa) prior to transitioning to a "hard gel" (G' > 1000 Pa) $\dot{Pa}$ ) with further increases in temperature. For all formulations,  $T_{\rm onset}$ was characterized as the temperature at which the slope of G' versus temperature exceeded 5 Pa/°C. These values aligned with soft gel formation within RP-containing samples. A complete rheological data set of G' and G'' as a function of temperature for molar ratios of 1:0, 1:0.5, 1:1, and 1:2 P407:RP is included in Figure S3. These curves were used to extract values for the gelation temperatures, maximum gel moduli, and gel moduli at body temperature for each formulation (Table S3). Strain amplitude sweeps of representative samples across the thermal transition confirmed that measurements were conducted near or within the linear viscoelastic regime (Figure S7).

Differential Scanning Calorimetry (DSC). The micellization of P407 and dehydration of RP chains were probed using a TA Instruments Q1000 DSC. Approximately 20  $\mu$ L of each formulation was loaded into hermetically sealed Tzero aluminum pans at room temperature. Following loading, samples were held at 7 °C for 10 min to ensure thermal equilibrium before being heated at 1 °C/min to 50 °C. For all samples, traces of heat flow as a function of temperature were normalized per gram sample and linearly baselined. For all formulations with a single peak in the endothermic trace, the total dehydration enthalpy ( $\Delta H_{\text{tot}}$ ) was equal to the dehydration enthalpy associated with the primary peak,  $\hat{\Delta}H_{\text{prim}}$ . Addition of certain RPs resulted in the appearance of a secondary shoulder in the trace at higher temperatures. In these cases, the primary peak was fit to an asymmetric double sigmoid and the area under this fit was used to extract  $\Delta H_{\text{prim}}$ , while the remaining area under the curve corresponded to the enthalpy of the shoulder region,  $\Delta H_{\rm s}$ . The traces and enthalpies of micellization for each formulation are included in Figure S13.

Small-Angle X-ray Scattering (SAXS). The micelle size and ordered packings were characterized as a function of temperature using small-angle X-ray scattering (SAXS). Synchrotron SAXS measurements were conducted at sector 12-ID-B at the Advanced Photon Source at Argonne National Laboratory. Samples were loaded into hermetically sealed DSC pans. Measurements with a 0.1 s exposure time were taken every 5 °C from 15 to 45 °C following a 10 min equilibration time at each temperature. Using a wavelength of  $\lambda$  =

0.886 Å and a sample-to-detector distance of 2.0 m, a q-range of 0.0035–0.9 Å $^{-1}$  was probed, where  $q=\frac{4\pi}{\lambda}\sin\frac{\theta}{2}$  in which  $\theta$  is the scattering angle. Two-dimensional scattering patterns were recorded using an Eiger2 S 9 M detector and azimuthally integrated following calibration with silver behenate to yield one-dimensional traces. The 1D data for each formulation as a function of temperature is included in Figures S15–S18, and representative 2D patterns are shown in Figure S19. Ordered cubic phases were identified by the location of Bragg peaks at characteristic positions of  $q/q^*=1$ ,  $\sqrt{4/3}$ ,  $\sqrt{8/3}$ ,  $\sqrt{11/3}$ , and 2 for face-centered cubic (FCC) and  $q/q^*=1$ ,  $\sqrt{2}$ ,  $\sqrt{3}$ , 2, and  $\sqrt{5}$  for body-centered cubic (BCC). The position of  $q^*$  was used to determine the lattice size, a. The micelle radius,  $R_p$  was approximated as half of the nearest neighbor distance within the respective lattices.

#### ■ RESULTS AND DISCUSSION

**Incorporation of 10R5.** Adding 10R5, a low molecular weight, high PEO-fraction RP, to 15% P407 solutions hinders the formation of a hard gel. For formulations containing 1:0.5, 1:1, and 1:2 P407:10R5, both G' and G'' monotonically increase above 28 °C, achieving values on the order of only  $10^2$  Pa or less by 50 °C (Figures 1b and S3); in contrast, all other

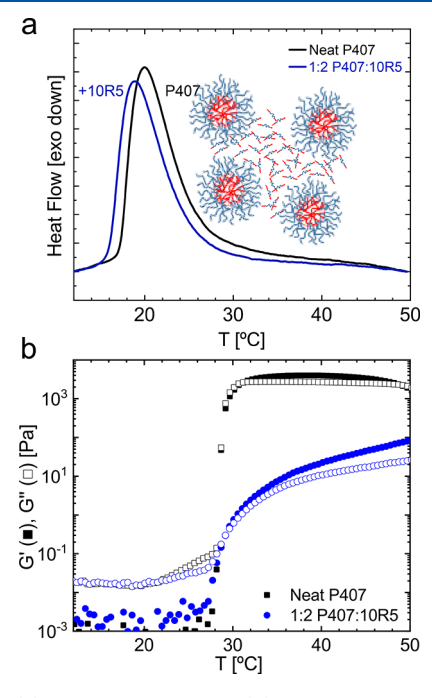


**Figure 1.** (a) DSC traces and (b) rheology with increasing temperature for neat P407 and P407 containing 1:2 10R5. Addition of 10R5 to P407 formulations hinders gelation, as RP chains do not incorporate into P407 micelles.

RP-containing systems achieve maximum moduli in the range of  $10^3-10^4$  Pa. Frequency sweeps conducted at discrete temperatures on formulations containing 1:2 P407:10R5 show the transformation from liquid to soft solid with increasing temperature (Figure S10). At 25 and 30 °C, the formulation displays liquidlike properties with G'' being greater than G' and scaling with  $\omega^1$ . With increasing temperature, G' exceeds G'' across all measured frequencies. While both G' and G'' are relatively frequency-independent across a range of high frequencies (>1 rad/s), at lower frequencies G' displays a downturn and G'' upturns. This behavior is similar to that

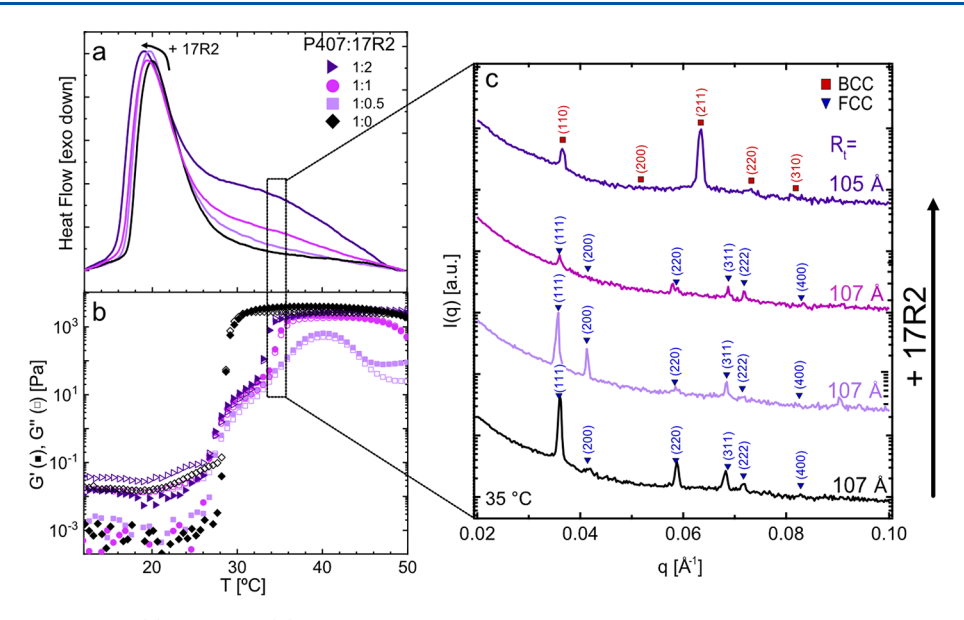


Figure 2. Temperature-dependent (a) DSC and (b) rheology show that the addition of increasing amounts of 17R2 to P407 micelles affects the micellization and gelation processes. (c) Corresponding 1D SAXS traces at 35 °C show a transition from FCC-to-BCC packed micelles upon addition of 17R2.

observed in jammed colloidal glasses and is likely due to micellar rearrangement at longer time scales. 58,59

These rheological results suggest that 15% P407 formulations with 10R5 have limited applicability due to the low modulus upon heating. In contrast, Liu et al. found that adding 10R5 to higher-concentration P407 solutions (20%) increases  $T_{\rm onset}$  but does not otherwise hinder hard gel formation, resulting in moduli in the kPa range, of comparable magnitude to those of neat P407 solutions. These differences are attributed to the change in P407 concentration, as additional studies on 18% P407 with 10R5 show a similar increase in  $T_{\rm onset}$  with added 10R5 and moduli comparable to those of neat P407 (Figure S14).

Despite its limited applicability within 15% P407 solutions, the incorporation of 10R5 can still be used to elucidate the underlying assembly mechanisms in other RP-containing formulations. The DSC traces of neat P407 solutions exhibit a single endothermic peak associated with the dehydration of the PPO block during micelle formation (Figures 1a and S13). Consistent with findings from more concentrated P407/10R5 formulations, 49 addition of 10R5 slightly decreases  $T_{\rm mic}$  but does not alter the DSC peak shape or width (Figure 1a). In addition to  $T_{\rm mic}$  the effect of RP addition on the enthalpy of micellization,  $\Delta H_{\text{tot}}$ , found from integrating under the DSC curve helps illuminate the process of RP incorporation. To properly compare  $\Delta H_{\mathrm{tot}}$  across formulations with different RP contents, values must be normalized to the concentration of PPO in each solution ( $\Delta H_{\text{tot,PPO}}$ ), as PPO dehydration drives these endothermic transitions. If all the PPO blocks in both P407 and the RP dehydrate to the same extent, then  $\Delta H_{\text{tot,PPO}}$ should be independent of RP content.<sup>47</sup> For 10R5, this independence is not observed; instead,  $\Delta H_{\text{tot,PPO}}$  decreases substantially upon increasing addition of 10R5 (Table S5). Interestingly, normalization to the number of PPO groups in P407 only results in  $\Delta H_{\text{tot,PPO}_{\text{P407}}}$  values that are uncorrelated with 10R5 content, with  $\Delta H_{\rm mic}$  = 88 versus 89 J/g PPO<sub>P407</sub> for 1:2 P407:10R5 and neat P407, respectively (Table S5). This analysis suggests that few, if any, PPO groups in 10R5 are dehydrated up to 50 °C and are thus unlikely to be

incorporated in the micelles. This result is unsurprising given the high aqueous solubility of 10R5, resulting from its low molecular weight (2.1 kDa) and high PEO weight fraction (52%) relative to the other RPs. Accordingly, the 10R5 unimers likely hinder gelation by preventing adjacent P407 micelles from significantly overlapping, as would be required for formation of a strong gel network (Figure 1b).<sup>49</sup>

Effect of PEO Molecular Weight on Assembly: 17R2 vs 17R4. In contrast to 10R5, adding increasing amounts of 17R2, an RP of similar molecular weight but higher PPO content (74 wt %), significantly alters the shape of the DSC traces (Figure 2a). Specifically, 17R2 addition results in the development of a high-temperature shoulder and broadening of the primary micellization peak. The higher PPO content of 17R2 relative to 10R5 decreases the RP solubility and drives PPO dehydration to lower temperatures. This widening of the primary peak paired with the appearance of a secondary shoulder indicates that 17R2 dehydration overlaps with the upper-temperature region of P407 micellization. Further, the total enthalpy of dehydration, including both the primary peak and shoulder,  $\Delta H_{\mathrm{tot,PPO}}$ , is similar across 17R2 concentrations  $(89 \text{ J/g}_{PPO,tot} \text{ for neat P407 vs } 92 \text{ J/g}_{PPO,tot} \text{ for } 1:2 \text{ P407:17R2}),$ suggesting a similar degree of dehydration for both the RP and P407 chains (see Table S5 for all  $\Delta H$  values).

As with 10R5, the dehydration mechanism dictates the rheological and structural transitions associated with the solution-to-gel transition. The tail of the primary peak and onset of the secondary shoulder correspond to the formation of a soft solid, similar to that observed in P407/10R5 solutions (Figure 2a,b). With increasing temperature, as more 17R2 chains dehydrate, this soft solid transitions to a higher-modulus gel (Figure 2b). Changes in 17R2 concentration affect  $G'_{\text{max}}$  in an irregular manner due to both micelle structure and polymer concentration effects. Similarly with 10R5, though to a lesser extent, addition of low fractions of 17R2 (1:0.5 P407:17R2) dramatically reduces  $G'_{\text{max}}$  relative to that of neat P407 (0.6 kPa vs 3.9 kPa). However, higher RP incorporations (1:1 and 1:2 P407:17R2) counteract this effect by increasing the overall polymer concentration in the solution, achieving maximum

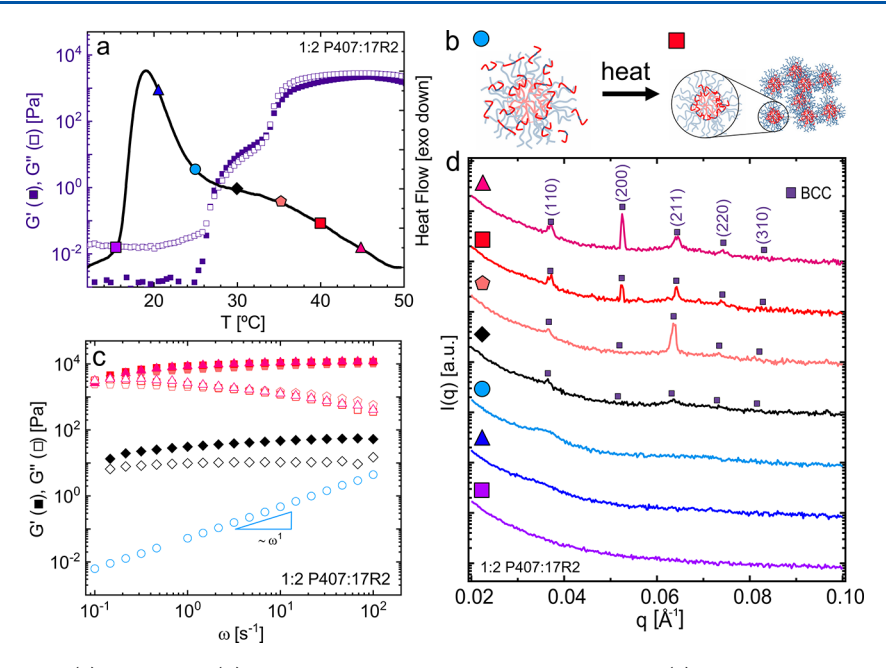
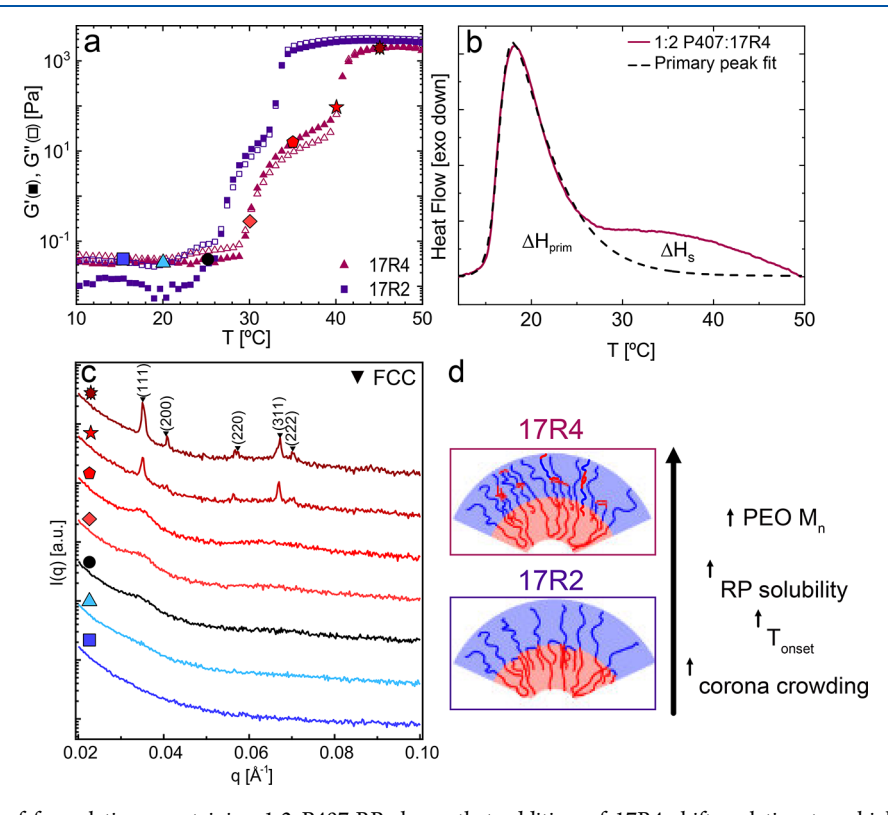


Figure 3. Rheology (a,c), DSC (a), and SAXS (d) for formulations containing 1:2 P407:17R2. (a) Temperature-dependent thermodynamic and rheological transitions measured via DSC and rheology on heating show a two-step incorporation mechanism upon 17R2 addition. (b) Schematics showing hypothesized RP incorporation mechanism. (c) Frequency sweeps at discrete temperatures (corresponding to symbols in a) across the liquid to soft gel to hard gel transitions. (d) SAXS measurements taken at the temperatures indicated by symbols on heating suggest the formation of BCC-packed micelles with increasing temperature.



**Figure 4.** (a) Rheology of formulations containing 1:2 P407:RP shows that addition of 17R4 shifts gelation to a higher temperature, but the gelation pathway is similar to that of formulations containing 17R2. (b) DSC trace of 1:2 P407:17R4 shows that the primary peak and secondary shoulder are well-separated from each other, indicating distinct dehydration processes. To illustrate this separation, the primary peak is fit to an asymmetric double sigmoid. (c) SAXS analyses of 1:2 17R4 solutions further show the shift of gelation to a higher temperature and the formation of an FCC packing, similar to that exhibited by neat P407 solutions. (d) Increasing the PEO molecular weight while keeping the PPO molecular weight constant results in an increase in the RP solubility,  $T_{\rm onset}$ , and crowding in the coronal region.

moduli of a similar order to those of neat P407. As with neat P407, these gels result from the arrangement of micelles into

cubic packings. Consistent with previous work on 31R1,<sup>47</sup> the addition of high concentrations of 17R2 (1:2 P407:17R2)

drive the formation of a body-centered cubic (BCC) over face-centered cubic (FCC) packing (Figure 2c). The 2D scattering patterns from these samples display a low overall intensity and are spotty, lacking isotropic rings (Figure S19). As a result of this spottiness, likely stemming from slow nucleation kinetics and large grain sizes, the intensity of each peak in the 1D traces are susceptible to variations in individual spot intensities.

SAXS with increasing temperature for 1:2 P407:17R2 formulations supports the mechanism of gradual 17R2 dehydration with increasing temperature and the formation of mixed micelles. At 30 °C (Figure 3b, diamond), SAXS suggests that the soft solid likely does not have strong longrange order, as the peaks corresponding to BCC packing are barely visible. At this temperature, nucleated ordered regions may coexist with disordered regions composed of 17R2 unimers similar to that reported by Castelletto et al.<sup>60</sup> Within this region, G' is greater than G'' across all measured frequencies but decreases slightly at low frequencies (Figure 3c). As position increases further, across the endothermic shoulder in the DSC curve (Figure 3a), more 17R2 chains are expected to dehydrate and incorporate into mixed micelles with P407. This incorporation coincides with a dramatic increase in the moduli and ordering of micelles into a betterdefined BCC packing. Frequency sweeps of 1:2 P407:17R2 within this higher-temperature regime indicate subtle differences in the relaxation behavior relative to neat P407 (Figures 3c and S9). While the dynamic moduli of neat P407 are relatively frequency-independent, with just a slight downturn in G' and upturn in G'' at low frequencies, addition of 17R2 results in a more dramatic frequency dependence, with G' and G'' converging at low frequencies.

While the molecular weight of the RP PPO block correlates with the temperature for chain dehydration, the corresponding PEO molecular weight also strongly influences this dehydration process and the resulting gelation temperature and gel structure, as is seen for 17R2 vs 17R4 (Figure 4). These two RPs have the same molecular weight of PPO, but the block fraction of PEO is much higher for 17R4 ( $x_{PEO} = 0.42 \text{ vs } 0.26$ ). As with 17R2, the addition of 17R4 leads to a reduction in the micellization temperature and the development of a hightemperature shoulder, particularly evident for 1:2 P407:17R4 (Figure 4b). In contrast to 17R2, the shoulder is shifted to higher temperatures and is well separated from the primary peak. This shift is likely due to the higher molecular weight of PEO in 17R4 that increases the overall hydrophilicity, even though 17R4 has the same PPO molecular weight as 17R2. Integrating the primary DSC peak suggests that only PPO blocks in P407, and not in 17R4, are dehydrating at this lower temperature. Here, the  $\Delta H_{\text{prim}}$  is comparable to that of neat P407 and independent of 17R4 content when the value is normalized to the mass of PPO in P407 only (see Table S5). Further,  $\Delta H_{\text{tot,PPO}}$  obtained from integrating the entire curve (primary peak plus secondary shoulder) and normalizing to the total PPO content decreases with increasing 17R4 content. Such behavior is in direct contrast to that observed with 17R2 and suggests that some of the 17R4 chains are not dehydrating to the same extent as the P407 chains over the measured temperature range.

The shift in 17R4 incorporation to higher temperatures and change in overall dehydration extent directly impacts the gelation temperature and gel morphology. While the rheology curve of the 1:2 P407:17R4 solution has a similar shape to that of 17R2-containing solutions, the transition is shifted  $\sim$ 5 °C to

higher temperatures and the "soft-gel" region at lower temperatures widens. The transition from a liquid to soft gel corresponds to an amplifying of the disordered micelle peaks in the 1D SAXS traces; however, ordering does not occur until the secondary rheological transition to the harder gel (Figure 4a,c). This secondary transition, which occurs slightly above physiological conditions, results in the formation of FCCpacked micelles, as is seen in neat P407 formulations. In comparison to the more-hydrophobic 17R2, which localizes closer to the micelle core, the higher PEO fraction in 17R4 likely allows for more localization of the reverse poloxamers in the coronal region (Figure 4d). This crowding limits the flexibility of coronal chains, which drives FCC packing over BCC. Interestingly, the FCC lattice parameter and resulting micelle radius, Rt, are also very similar to those of neat P407 (109 Å for 1:2 P407:17R4 vs 107 Å for neat P407). As the formulation is in the soft-gel regime at body temperature, adding 17R4 is unlikely to be useful for enhancing gel moduli for drug delivery at this P407 concentration, in contrast to adding the longer RP 25R4, which enhances the moduli vs that for neat P407 via bridging. 47,49,56,61 However, addition of hydrophobic drugs often shifts the gelation to undesirably low temperatures, 9,29,30,47,62 and incorporation of an RP such as 17R4 has the potential to increase the gelation temperature without substantially altering the final gel structure.

Despite similarities in the micelle size and packing between neat P407 and 1:2 P407:17R4 (both FCC), addition of 17R4 alters the relaxation processes within the higher-temperature formulations, resulting in G' and G'' converging at low frequencies (Figure S11). Previously Li and Hyun used strain amplitude sweeps to investigate gels composed of 25% P407 with various concentrations and molecular weights of PEO homopolymer.<sup>63</sup> While neat P407 gels display a clear maximum in G'' during microstructural breakup, they found that addition of PEO homopolymer dampened this peak amplitude, likely due to a reduction in the strength of the close-packed structures within the gels due to the PEO homopolymer presence within the corona region. Interestingly, addition of 17R4 has a similar effect, reducing the amplitude of the G'' peak and decreasing the strain at which G' and G'' cross each other relative to neat P407 and formulations containing other RPs. These differences, coupled with the similar SAXS traces, support that 17R4 incorporates primarily into the coronal region.

Impact of PPO Molecular Weight on Assembly: 17R2 vs 25R2. In addition to block fraction, the molecular weight of the PPO block also strongly impacts solubility, with higher molecular weight PPO blocks reducing the solubility of RP chains. In comparison to 17R2, 25R2 has approximately the same block fractions but a significantly higher molecular weight (Table 1). As expected, this decrease in solubility shifts dehydration of 25R2 PPO blocks to lower temperatures, as indicated by a broad endothermic peak in the DSC traces that increases in width with 25R2 addition (Figures 5 and S13). While no distinct shoulder can be separated from the primary peak, as could be done with 17R4, the peak is asymmetric, with a significant high-temperature tail. This feature is likely due to the slightly lower molecular weight of PPO in 25R2 than in P407 (2.5 kDa vs 3.4 kDa). Presumably the micelles at low temperatures are composed primarily of P407 with a limited number of 25R2 chains, whereas the fraction of dehydrated 25R2 in each micelle increases with temperature. As with 17R2,  $\Delta H_{\text{tot}}$  normalized by the total mass of PPO in both P407

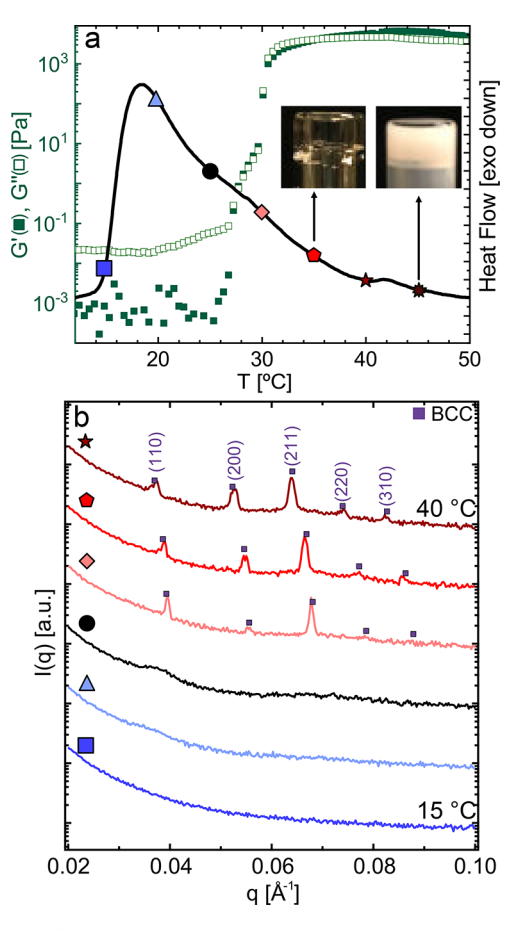


**Figure 5.** (a) Rheology and DSC for formulations containing 1:2 P407:25R2 suggest the formation of mixed P407/25R2 micelles. Increases in temperature decrease the 25R2 solubility, resulting in eventual macrophase separation at high 25R2 loadings. (b) Corresponding SAXS shows the formation of BCC-packed micelles upon gelation.

and 25R2 is uncorrelated with 25R2 content and approximately equal to that of neat P407, indicating that all PPO units dehydrate to a similar extent, albeit at different temperatures (Table S5).

The decreased RP solubility relative to 17R2 also decreases the temperature range at which the soft gel is present prior to stronger gel formation. For formulations with 1:2 P407:17R2, this region persists for 8 °C in comparison to only 2 °C for 1:2 P407:25R2. As with 17R2, low molar ratios of 25R2 slightly reduce  $G'_{\rm max}$  relative to neat P407 (3.9 kPa for neat P407, 2.2 kPa for 1:0.5, and 3.1 kPa for 1:1); however, the effect is much less pronounced than with 17R2 (Figure S3b,d). Further, addition of 1:2 P407:25R2 results in a gel with a higher  $G'_{\rm max}$  than neat P407 (6.7 kPa). These increases are similar to those observed previously upon addition of 31R1 and can likely be attributed to the increase in micelle volume fraction in solution due to RP incorporation. <sup>47</sup>

As with the other low-PEO-content RPs, the dehydrated 25R2 chains are expected to reside predominantly within the core, near the interfacial region, due to the high PPO fraction. As temperature is increased across the broad endothermic transition, formulations with a low quantity of 25R2 (1:0.5) order into an FCC packing, while higher 25R2 contents drive a BCC packing (Figures 5 and S17). Such an FCC-to-BCC transition, as was observed for 17R2 and

previously for 31R1,47 supports a localization of RPs in the core region and a reduction in the density of the coronal chains. With increasing temperature, R<sub>t</sub> increases substantially, as evidenced by the shift of  $q^*$  to lower values, with  $R_t$  equaling 96 Å at 30  $^{\circ}$ C to 104 Å at 40  $^{\circ}$ C. The observed increase in lattice size across the broad endothermic transition is consistent with the idea of delayed insertion of 25R2 chains, which expands the total micelle size. Such an expansion is likely not visible in the 17R2 formulations because RPs were added on a molar basis and therefore the incorporated volume fraction of 17R2 is significantly lower than that of 25R2 due to the lower molecular weight. This idea is consistent with the fact that a lesser extent of swelling is observed upon incorporation of lower molar ratios of 25R2 (Figure S17). Mixed micelles, such as those formed from low-solubility RPs, can improve the bioavailability of drugs released from gels. 65-67 The addition of 25R2 therefore provides a potential mechanism to improve drug diffusion without changing gel properties that are necessary for the desired application. Unfortunately, the low solubility of 25R2 also affects the stability of the gel at elevated temperatures. At conditions just above body temperature, a small endothermic peak is seen in the DSC curve. Visual observations indicate that this transition is accompanied by clouding, as the solubility limit of 25R2 within this system is reached and macrophase separation occurs.47,68

Guidelines for Hydrogel Design. Precise control over the gelation temperature is essential for effective targeted drug delivery. For example, certain applications dictate that formulations be a liquid at room temperature to facilitate ease of injection but gel rapidly upon contact with warm skin or the tympanic membrane. The findings of this study paired with prior work<sup>47</sup> on two larger RPs (31R1 and 25R4) suggest that the gelation temperature and modulus can be tuned by adding specific RPs to P407 (Figures 6 and S3). Generally, higher molecular weight RPs (25R2, 25R4, 31R1) increase  $G'_{\text{max}}$  relative to that of neat P407 when added in sufficient molar ratios (Figures S3 and S5), $^{47}$  whereas lower  $M_n$  RPs (10R5, 17R2, and 17R4) reduce  $G'_{\text{max}}$ . Additionally, the aqueous solubility of each RP, dictated by the molecular weight and block fraction of PPO, can be used to tune the gelation temperatures of these formulations. Decreasing the RP solubility results in a decrease in the temperature of hard gel formation,  $T_{\text{hard gel}}$ , defined as when  $G' > 10^3 \text{ Pa}$  (Figures 6b) and S6). The molar ratio at which the RP is added also has an effect on gelation with higher RP amounts typically having a more dramatic effect on  $T_{\rm hard\ gel}$  than lower amounts. Importantly, the combination of RP molecular weight and block fraction differences can be used to target specific gelation temperatures and moduli. For example, addition of high PEOcontent RPs such as 10R5, 17R4, and 25R4 all delay the onset of gel formation, while the different molecular weights of these RPs dictate the gel modulus. These specific RPs remain hydrated in solution at temperatures above the P407 micellization transition due to their high PEO contents and relatively low molecular weights, preventing a strong interconnected micelle network from forming until higher temperatures. While adding 10R5 to 15% P407 prevents a strong gel from forming, this RP may be useful in applications where tuning the thermal response is more critical than obtaining a strong hydrogel; additionally, when added to larger quantities of P407 or in conjunction with other RPs, 10R5 may

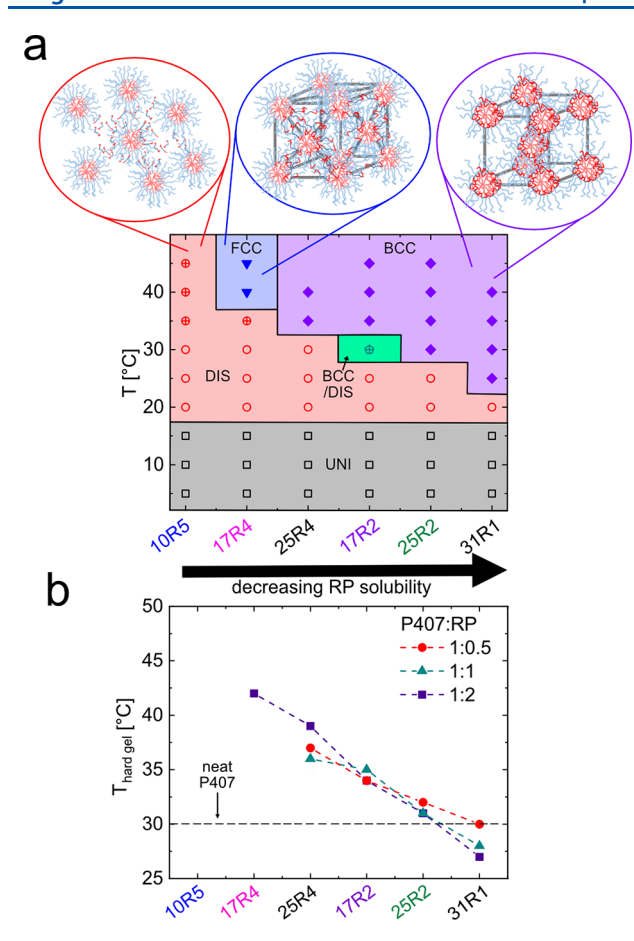


**Figure 6.** (a) Morphology as a function of temperature for formulations containing 1:2 P407:RP. Increasing either PPO molecular weight or block fraction decreases relative RP solubility, favoring a lower gelation temperature and a BCC micelle packing within the gel. UNI = unimers; DIS = disordered micelles; FCC = face-centered cubic; BCC = body-centered cubic. Open = liquid, crossed = soft gel (10–1000 Pa), filled = hard gel (>1000 Pa). Morphology was determined via SAXS, measured every 5 °C. The unimer-to-disordered micelle transition was also determined using DSC. (b) Hard gel transition temperature as a function of RP identity and amount.

provide a straightforward route for finely tuning the hydrogel thermoresponsiveness.

In addition to tuning gelation temperature and modulus, RPs can be used to alter gel microstructure (Figure 6a). For example, high PPO-content RPs are anticipated to localize near the core and interfacial region, forming mixed micelles with P407. These mixed micelles have a lower density of coronal chains than neat P407 micelles have. This reduction in chain density favors BCC over FCC, 69-74 as occurs when pure PPO or other poloxamers comicellize near P407 micelle Such differences in RP localization can be harnessed to optimize formulations for specific applications. For example, certain formulations require improving drug encapsulation and flux without drastically altering the gel properties or gelation temperature. Previously, mixed micelles composed of two different poloxamers or surfactants have been shown to improve drug loading and bioavailability due to the nonuniformity or lower density of chains in the corona region. 65-67 Further, Buxton et al. showed computationally that drug diffusion from micelle cores is improved in systems with a lower chain density in the coronal region. Hence,

addition of high-PPO content RPs to P407 provides a pathway toward improving drug flux.

Alternatively, certain applications, such as protein immobilization and protection, require a crowded environment. Higher PEO-content RPs, such as 10R5 and 17R4, localize more in the coronal region than do lower PEO-content RPs. This localization decreases the mobility of corona chains, potentially providing a more supportive environment for proteins.

While these results provide insight and design guidelines for developing P407 drug-delivery hydrogels with tunable thermal gelation temperatures and moduli, the mechanical and structural properties of each hydrogel will depend on the precise formulation parameters, including the volume fraction of P407 and RP and the type and quantity of small molecules employed. While the bare P407 and RP systems described herein did not contain small molecules, prior work on bare P407 with added 31R1 or 25R4 suggested a similar mechanism of RP incorporation in the presence of small molecules; however, quantitative parameters like the gelation temperature, micelle size, or maximum modulus differed with small-molecule incorporation. 47

#### CONCLUSION

Addition of reverse poloxamers to aqueous P407 solutions at a constant concentration alters the gelation temperatures, gel moduli, and resulting microstructures. In particular, the solubility of various RPs, dictated both by the molecular weight of the PPO block and the block fraction, determines the dehydration mechanism and resulting gelation temperature. Low-solubility RPs, such as 17R2, 25R2, and 31R1, form mixed micelles with P407, localizing near the core of the micelle. These mixed micelles have the potential to increase drug diffusion and bioavailability. Increasing PPO molecular weight decreases the RP-incorporation temperature, with 17R2 dehydrating in a distinct second step after P407 dehydration, 25R2 at slightly elevated temperatures compared to P407, and 31R1 dehydrating at the same temperature as P407. Therefore, high PPO-content RPs can be used as additives to alter the gelation temperature while also promoting drug diffusion due to the lower chain density in the corona region.

In contrast, higher PEO-fraction RPs have a much higher solubility in water. Addition of 10R5 prevents the formation of a strong gel, as the RP remains in solution and sterically blocks interactions between micelles. Increasing PPO molecular weight (17R4 and 25R4) decreases RP solubility, such that a gel is able to form at elevated temperatures. Hence, RPs serve as primary tools for altering gelation temperature for targeted applications. Further, the longer PEO chains enable these RPs to localize more in the corona region, vis-à-vis the higher PPOcontent counterparts. This corona localization decreases chain mobility within the corona, which may be beneficial for certain applications, including protein immobilization. By addition of commercially available reverse poloxamers to P407 formulations, the gelation temperature and gel modulus can be independently tuned, providing fine control over the structure and dynamics of these nontoxic thermoresponsive hydrogels for applications in medicine and beyond.

#### ASSOCIATED CONTENT

#### **Supporting Information**

The Supporting Information is available free of charge at https://pubs.acs.org/doi/10.1021/acs.langmuir.3c00088.

Size-exclusion chromatography and NMR on each RP, rheology, SAXS, and DSC temperature ramps for all formulations, and frequency and amplitude sweeps for select formulations (PDF)

#### AUTHOR INFORMATION

#### **Corresponding Author**

Michelle A. Calabrese – Department of Chemical Engineering and Materials Science, University of Minnesota, Minneapolis, Minnesota 55455, United States; orcid.org/0000-0003-4577-6999; Email: mcalab@umn.edu

#### **Authors**

Joanna M. White — Department of Chemical Engineering and Materials Science, University of Minnesota, Minneapolis, Minnesota 55455, United States; orcid.org/0000-0002-5323-4332

Ally Garza – Department of Health and Biomedical Sciences, University of Texas Rio Grande Valley, Edinburg, Texas 78539, United States

James J. Griebler — Department of Chemical and Biomolecular Engineering, University of Illinois Urbana—Champaign, Urbana, Illinois 61801, United States; orcid.org/0000-0002-1056-4593

Frank S. Bates — Department of Chemical Engineering and Materials Science, University of Minnesota, Minneapolis, Minnesota 55455, United States; Oorcid.org/0000-0003-3977-1278

Complete contact information is available at: https://pubs.acs.org/10.1021/acs.langmuir.3c00088

#### Notes

The authors declare no competing financial interest.

#### ACKNOWLEDGMENTS

Research reported in this publication was supported by the National Institute on Deafness and Other Communication Disorders of the National Institutes of Health under Award R21DC019184-01A1. Researchers contributing to this work were additionally supported by the National Science Foundation (NSF) Graduate Research Fellowship under Grant CON-75851, Project 00074041 (J.M. White), and through the Partnership for Research and Education in Materials (PREM) Program of the National Science Foundation under Award DMR-2122178 and the University of Minnesota MRSEC under Award Number DMR-2011401 (A. Garza). Any opinions, findings, and conclusions or recommendations expressed in this material are those of the author(s) and do not necessarily reflect the views of the National Science Foundation. This research used resources of the Advanced Photon Source, a U.S. Department of Energy (DOE) Office of Science User Facility, operated for the DOE Office of Science by Argonne National Laboratory under Contract DE-AC02-06CH11357. SAXS experiments were carried out at Sector 12-ID-B of the Advanced Photon Source. Lab-source SAXS experiments were carried out at the Characterization Facility, University of Minnesota, which receives partial support from the NSF through the MRSEC (Award Number DMR-2011401) and the NNCI (Award ECCS-2025124) programs. The authors thank the Anton Paar VIP program for the rheometer used in this work. NMR instruments used to collect data reported in this publication

were purchased and maintained with support from the Office of the Vice President of Research, College of Science and Engineering, and the Department of Chemistry at the University of Minnesota.

#### REFERENCES

- (1) Huynh, C. T.; Nguyen, M. K.; Lee, D. S. Injectable block copolymer hydrogels: achievements and future challenges for biomedical applications. *Macromolecules* **2011**, *44*, 6629–6636.
- (2) Bellotti, E.; Schilling, A. L.; Little, S. R.; Decuzzi, P. Injectable thermoresponsive hydrogels as drug delivery system for the treatment of central nervous system disorders: A review. *J. Controlled Release* **2021**, 329, 16–35.
- (3) Fan, R.; Cheng, Y.; Wang, R.; Zhang, T.; Zhang, H.; Li, J.; Song, S.; Zheng, A. Thermosensitive Hydrogels and Advances in Their Application in Disease Therapy. *Polymers* **2022**, *14*, 2379.
- (4) Cui, N.; Dai, C.-Y.; Mao, X.; Lv, X.; Gu, Y.; Lee, E.-S.; Jiang, H.-B.; Sun, Y. Poloxamer-Based Scaffolds for Tissue Engineering Applications: A Review. *Gels* **2022**, *8*, 360.
- (5) Yang, X.; Yang, R.; Chen, M.; Zhou, Q.; Zheng, Y.; Lu, C.; Bi, J.; Sun, W.; Huang, T.; Li, L.; et al. KGF-2 and FGF-21 poloxamer 407 hydrogel coordinates inflammation and proliferation homeostasis to enhance wound repair of scalded skin in diabetic rats. *BMJ. Open Diabetes Research and Care* 2020, 8, e001009.
- (6) Cao, F.; Zhang, X.; Ping, Q. Drug Delivery New method for ophthalmic delivery of azithromycin by poloxamer/Carbopol-based in situ gelling system. *Drug Delivery* **2010**, *17*, 500–507.
- (7) Grimaudo, M. A.; Pescina, S.; Padula, C.; Santi, P.; Concheiro, A.; Alvarez-Lorenzo, C.; Nicoli, S. Poloxamer 407/TPGS Mixed Micelles as Promising Carriers for Cyclosporine Ocular Delivery. *Mol. Pharmaceutics* **2018**, *15*, 571–584.
- (8) Kurniawansyah, I. S.; Rusdiana, T.; Sopyan, I.; Ramoko, H.; Wahab, H. A.; Subarnas, A. In situ ophthalmic gel forming systems of poloxamer 407 and hydroxypropyl methyl cellulose mixtures for sustained ocular delivery of chloramphenicole: optimization study by factorial design. *Heliyon* **2020**, *6*, e05365.
- (9) Yang, R.; Sabharwal, V.; Okonkwo, O. S.; Shlykova, N.; Tong, R.; Lin, L. Y.; Wang, W.; Guo, S.; Rosowski, J. J.; Pelton, S. I.; Kohane, D. S.; et al. Treatment of otitis media by transtympanic delivery of antibiotics. *Science translational medicine* **2016**, *8*, 356ra120.
- (10) Yang, R.; Sabharwal, V.; Shlykova, N.; Okonkwo, O. S.; Pelton, S. I.; Kohane, D. S. Treatment of Streptococcus pneumoniae otitis media in a chinchilla model by transtympanic delivery of antibiotics. *JCI Insight* **2018**, 3, 1–10.
- (11) Yang, R.; Okonkwo, O. S.; Zurakowski, D.; Kohane, D. S. Synergy between chemical permeation enhancers and drug permeation across the tympanic membrane. *J. Controlled Release* **2018**, 289, 94–101.
- (12) Edmunds, A. L. Otiprio: An FDA-approved ciprofloxacin suspension gel for pediatric otitis media with effusion. *Pharm. Ther.* **2017**, 42, 307.
- (13) Wang, W.; Wat, E.; Hui, P. C. L.; Chan, B.; Ng, F. S. F.; Kan, C.-W.; Wang, X.; Hu, H.; Wong, E. C. W.; Lau, C. B. S.; Leung, P.-C. Dual-functional transdermal drug delivery system with controllable drug loading based on thermosensitive poloxamer hydrogel for atopic dermatitis treatment. *Sci. Rep.* **2016**, *6*, 1–10.
- (14) Tobin, K. V.; Fiegel, J.; Brogden, N. K. Thermosensitive gels used to improve microneedle-assisted transdermal delivery of naltrexone. *Polymers* **2021**, *13*, 933.
- (15) Patel, M.; Lee, H. J.; Park, S.; Kim, Y.; Jeong, B. Injectable thermogel for 3D culture of stem cells. *Biomaterials* **2018**, *159*, 91–107.
- (16) Ye, K.; Wang, X.; Cao, L.; Li, S.; Li, Z.; Yu, L.; Ding, J. Matrix stiffness and nanoscale spatial organization of cell-adhesive ligands direct stem cell fate. *Nano Lett.* **2015**, *15*, 4720–4729.
- (17) Buxton, G. A.; Clarke, N. Drug diffusion from polymer coreshell nanoparticles. *Soft Matter* **2007**, *3*, 1513–1517.

- (18) Ping, G.; Yuan, J.-M.; Sun, Z.; Wei, Y. Studies of effects of macromolecular crowding and confinement on protein folding and protein stability. *Journal of Molecular Recognition* **2004**, *17*, 433–440.
- (19) Dao, M. M.; Domach, M. M.; Walker, L. M. Impact of dispersed particles on the structure and shear alignment of block copolymer soft solids. *J. Rheol.* **2017**, *61*, 237–252.
- (20) Despa, F.; Orgill, D. P.; Lee, R. C. Effects of crowding on the thermal stability of heterogeneous protein solutions. *Annals of biomedical engineering* **2005**, 33, 1125–1131.
- (21) Nandy, A.; Chakraborty, S.; Nandi, S.; Bhattacharyya, K.; Mukherjee, S. Structure, activity, and dynamics of human serum albumin in a crowded pluronic F127 hydrogel. *J. Phys. Chem. B* **2019**, 123, 3397–3408.
- (22) Mustafi, D.; Smith, C. M.; Makinen, M. W.; Lee, R. C. Multi-block poloxamer surfactants suppress aggregation of denatured proteins. *Biochimica et Biophysica Acta (BBA)-General Subjects* **2008**, 1780, 7–15.
- (23) Pitto-Barry, A.; Barry, N. P. Pluronic® block-copolymers in medicine: from chemical and biological versatility to rationalisation and clinical advances. *Polym. Chem.* **2014**, *5*, 3291–3297.
- (24) Zhang, C.; Zhang, J.; Qin, Y.; Song, H.; Huang, P.; Wang, W.; Wang, C.; Li, C.; Wang, Y.; Kong, D. Co-delivery of doxorubicin and pheophorbide A by pluronic F127 micelles for chemo-photodynamic combination therapy of melanoma. *J. Mater. Chem. B* **2018**, *6*, 3305–3314.
- (25) Fares, A. R.; ElMeshad, A. N.; Kassem, M. A. A. Enhancement of dissolution and oral bioavailability of lacidipine via pluronic P123/F127 mixed polymeric micelles: formulation, optimization using central composite design and in vivo bioavailability study. *Drug Delivery* 2018, 25, 132–142.
- (26) Abdeltawab, H.; Svirskis, D.; Boyd, B. J.; Hill, A.; Sharma, M. Injectable thermoresponsive gels offer sustained dual release of bupivacaine hydrochloride and ketorolac tromethamine for up to two weeks. *Int. J. Pharm.* **2021**, *604*, 120748.
- (27) Torchilin, V. P. Structure and design of polymeric surfactant-based drug delivery systems. *J. Controlled Release* **2001**, 73, 137–172.
- (28) Tundisi, L. L.; Yang, R.; Borelli, L. P. P.; Alves, T.; Mehta, M.; Chaud, M. V.; Mazzola, P. G.; Kohane, D. S. Enhancement of the mechanical and drug-releasing properties of poloxamer 407 hydrogels with casein. *Pharm. Res.* **2021**, *38*, 515–522.
- (29) Djekic, L.; Čalija, B.; Medarević, O. Gelation behavior, drug solubilization capacity and release kinetics of poloxamer 407 aqueous solutions: The combined effect of copolymer, cosolvent and hydrophobic drug. *J. Mol. Liq.* 2020, 303, 112639.
- (30) Dumortier, G.; Grossiord, J. L.; Agnely, F.; Chaumeil, J. C. A review of poloxamer 407 pharmaceutical and pharmacological characteristics. *Pharm. Res.* **2006**, 23, 2709–2728.
- (31) Jain, D.; Kumar, V.; Singh, S.; Mullertz, A.; Bar-Shalom, D. Newer trends in in situ gelling systems for controlled ocular drug delivery. *J. Anal. Pharm. Res.* **2016**, *2*, 00022.
- (32) Ricci, E. J.; Bentley, M. V.; Farah, M.; Bretas, R. E.; Marchetti, J. M. Rheological characterization of Poloxamer 407 lidocaine hydrochloride gels. *Eur. J. Pharm. Sci.* **2002**, *17*, 161–167.
- (33) U.S. Food & Drug Administration: Inactive Ingredient Search for Approved Drug Products. https://www.accessdata.fda.gov/scripts/cder/iig/index.cfm (accessed March 21, 2023).
- (34) Giuliano, E.; Paolino, D.; Fresta, M.; Cosco, D. Mucosal applications of poloxamer 407-based hydrogels: An overview. *Pharmaceutics* **2018**, *10*, 159.
- (35) Wanka, G.; Hoffmann, H.; Ulbricht, W. Phase diagrams and aggregation behavior of poly(oxyethylene)-poly(oxypropylene)-poly(oxyethylene) triblock copolymers in aqueous solutions. *Macromolecules* **1994**, 27, 4145–4159.
- (36) Basak, R.; Bandyopadhyay, R. Encapsulation of hydrophobic drugs in Pluronic F127 micelles: effects of drug hydrophobicity, solution temperature, and pH. *Langmuir* **2013**, *29*, 4350–4356.
- (37) Ci, L.; Huang, Z.; Liu, Y.; Liu, Z.; Wei, G.; Lu, W. Aminofunctionalized poloxamer 407 with both mucoadhesive and

- thermosensitive properties: preparation, characterization and application in a vaginal drug delivery system. Acta Pharm. Sin. B 2017, 7, 593.
- (38) Akkari, A. C.; Papini, J. Z.; Garcia, G. K.; Franco, M. K.; Cavalcanti, L. P.; Gasperini, A.; Alkschbirs, M. I.; Yokaichyia, F.; De Paula, E.; Tófoli, G. R.; De Araujo, D. R. Poloxamer 407/188 binary thermosensitive hydrogels as delivery systems for infiltrative local anesthesia: Physico-chemical characterization and pharmacological evaluation. *Mater. Sci. Eng., C* 2016, 68, 299–307.
- (39) Wu, X.; Ge, W.; Shao, T.; Wu, W.; Hou, J.; Cui, L.; Wang, J.; Zhang, Z. Enhancing the oral bioavailability of biochanin A by encapsulation in mixed micelles containing Pluronic F127 and Plasdone S630. *Int. J. Nanomedicine* **2017**, *12*, 1475–1483.
- (40) Ruel-Gariépy, E.; Leroux, J.-C. In situ-forming hydrogels—review of temperature-sensitive systems. *Eur. J. Pharm. Biopharm.* **2004**, 58, 409–426.
- (41) Mortensen, K.; Brown, W. Poly(ethylene oxide)-poly(propylene oxide)-poly(ethylene oxide) triblock copolymers in aqueous solution. The influence of relative block size. *Macromolecules* **1993**, *26*, 4128–4135.
- (42) Parekh, P.; Dey, J.; Kumar, S.; Nath, S.; Ganguly, R.; Aswal, V.; Bahadur, P. Butanol solubilization in aqueous F127 solution: investigating the enhanced micellar solvation and consequent improvement in gelation characteristics. *Colloids Surf. B: Biointerfaces* **2014**, *114*, 386–391.
- (43) Alexandridis, P.; Holzwarth, J. F.; Hatton, T. A. Micellization of poly(ethylene oxide)-poly(propylene oxide)-poly(ethylene oxide) triblock copolymers in aqueous solutions: thermodynamics of copolymer association. *Macromolecules* **1994**, *27*, 2414–2425.
- (44) Cook, M. T.; Haddow, P.; Kirton, S. B.; McAuley, W. J. Polymers exhibiting lower critical solution temperatures as a route to thermoreversible gelators for healthcare. *Adv. Funct. Mater.* **2021**, *31*, 2008123.
- (45) Bohorquez, M.; Koch, C.; Trygstad, T.; Pandit, N. A study of the temperature-dependent micellization of pluronic F127. *J. Colloid Interface Sci.* 1999, 216, 34–40.
- (46) Shriky, B.; Kelly, A.; Isreb, M.; Babenko, M.; Mahmoudi, N.; Rogers, S.; Shebanova, O.; Snow, T.; Gough, T. Pluronic F127 thermosensitive injectable smart hydrogels for controlled drug delivery system development. *J. Colloid Interface Sci.* **2020**, *565*, 119–130
- (47) White, J. M.; Calabrese, M. A. Impact of small molecule and reverse poloxamer addition on the micellization and gelation mechanisms of poloxamer hydrogels. *Colloids Surf., A* **2022**, *638*, 128246.
- (48) Boonlai, W.; Tantishaiyakul, V.; Hirun, N.; Sangfai, T.; Suknuntha, K. Thermosensitive poloxamer 407/poly(acrylic acid) hydrogels with potential application as injectable drug delivery system. *AAPS PharmSciTech* 2018, 19, 2103–2117.
- (49) Liu, S.; Bao, H.; Li, L. Role of PPO-PEO-PPO triblock copolymers in phase transitions of a PEO-PPO-PEO triblock copolymer in aqueous solution. *Eur. Polym. J.* **2015**, *71*, 423–439.
- (50) Xie, Y.; Tang, J.; Lu, Z.; Sun, Z.; An, L. Effects of poly(propylene oxide)-poly(ethylene oxide)-poly(propylene oxide) triblock copolymer on the gelation of poly(ethylene oxide)-poly(propylene oxide)-poly(ethylene oxide) aqueous solutions. *J. Macromol. Sci. B* **2013**, *52*, 1183–1197.
- (51) Kojarunchitt, T.; Hook, S.; Rizwan, S.; Rades, T.; Baldursdottir, S. Development and characterisation of modified poloxamer 407 thermoresponsive depot systems containing cubosomes. *International journal of pharmaceutics* **2011**, 408, 20–26.
- (52) D'Errico, G.; Paduano, L.; Khan, A. Temperature and concentration effects on supramolecular aggregation and phase behavior for poly (propylene oxide)-b-poly (ethylene oxide)-b-poly (propylene oxide) copolymers of different composition in aqueous mixtures, 1. *J. Colloid Interface Sci.* **2004**, *279*, 379–390.
- (53) Zhou, Z.; Chu, B. Phase behavior and association properties of poly(oxypropylene)-poly(oxyethylene)-poly(oxypropylene) triblock copolymer in aqueous solution. *Macromolecules* **1994**, 27, 2025–2033.

- (54) Patel, T.; Bahadur, P.; Mata, J. The clouding behaviour of PEO-PPO based triblock copolymers in aqueous ionic surfactant solutions: a new approach for cloud point measurements. *J. Colloid Interface Sci.* **2010**, 345, 346–350.
- (55) Mortensen, K.; Brown, W.; Joergensen, E. Phase behavior of poly (propylene oxide)-poly (ethylene oxide)-poly (propylene oxide) triblock copolymer melt and aqueous solutions. *Macromolecules* **1994**, 27, 5654–5666.
- (56) Wang, Q.; Li, L.; Jiang, S. Effects of a PPO-PEO-PPO triblock copolymer on micellization and gelation of a PEO-PPO-PEO triblock copolymer in aqueous solution. *Langmuir* **2005**, *21*, 9068–9075.
- (57) Kojarunchitt, T.; Baldursdottir, S.; Dong, Y.-D.; Boyd, B. J.; Rades, T.; Hook, S. Modified thermoresponsive Poloxamer 407 and chitosan sol–gels as potential sustained-release vaccine delivery systems. *Eur. J. Pharm. Biopharm.* **2015**, *89*, 74–81.
- (58) Suman, K.; Sourav, S.; Joshi, Y. M. Rheological signatures of gel-glass transition and a revised phase diagram of an aqueous triblock copolymer solution of Pluronic F127. *Phys. Fluids* **2021**, 33, 073610
- (59) Winter, H. H. Glass transition as the rheological inverse of gelation. *Macromolecules* **2013**, *46*, 2425–2432.
- (60) Castelletto, V.; Hamley, I.; Yuan, X.-F.; Kelarakis, A.; Booth, C. Structure and rheology of aqueous micellar solutions and gels formed from an associative poly(oxybutylene)—poly(oxyethylene)—poly(oxybutylene) triblock copolymer. *Soft Matter* **2005**, *1*, 138–145.
- (61) Liu, S.; Li, L. Molecular interactions between PEO-PPO-PEO and PPO-PEO-PPO triblock copolymers in aqueous solution. *Colloids Surf. A: Physicochem. Eng. Asp.* **2015**, 484, 485–497.
- (62) Yong, C. S.; Choi, J. S.; Quan, Q. Z.; Rhee, J. D.; Kim, C. K.; Lim, S. J.; Kim, K. M.; Oh, P. S.; Choi, H. G. Effect of sodium chloride on the gelation temperature, gel strength and bioadhesive force of poloxamer gels containing diclofenac sodium. *Int. J. Pharm.* **2001**, 226, 195–205.
- (63) Li, X.; Hyun, K. Rheological study of the effect of polyethylene oxide (PEO) homopolymer on the gelation of PEO-PPO-PEO triblock copolymer in aqueous solution. *Korea-Australia Rheology Journal* **2018**, *30*, 109–125.
- (64) Pérez-Sánchez, G.; Vicente, F. A.; Schaeffer, N.; Cardoso, I. S.; Ventura, S. P.; Jorge, M.; Coutinho, J. Rationalizing the phase behavior of triblock copolymers through experiments and molecular simulations. *J. Phys. Chem. C* **2019**, *123*, 21224–21236.
- (65) Xu, H.; Yang, P.; Ma, H.; Yin, W.; Wu, X.; Wang, H.; Xu, D.; Zhang, X. Amphiphilic block copolymers-based mixed mixelles for noninvasive drug delivery. *Drug Delivery* **2016**, *23*, 3063–3071.
- (66) Patil, S.; Choudhary, B.; Rathore, A.; Roy, K.; Mahadik, K. Enhanced oral bioavailability and anticancer activity of novel curcumin loaded mixed micelles in human lung cancer cells. *Phytomedicine* **2015**, 22, 1103–1111.
- (67) Fares, A. R.; ElMeshad, A. N.; Kassem, M. A. Enhancement of dissolution and oral bioavailability of lacidipine via pluronic P123/F127 mixed polymeric micelles: formulation, optimization using central composite design and in vivo bioavailability study. *Drug delivery* 2018, 25, 132–142.
- (68) McCauley, P.; Kumar, S.; Calabrese, M. Criteria governing rod formation and growth in nonionic polymer wormlike micelles. *Langmuir* **2021**, *37*, 11676–11687.
- (69) Hirun, N.; Tantishaiyakul, V.; Sangfai, T.; Boonlai, W.; Soontaranon, S.; Rugmai, S. The effect of poly(acrylic acid) on temperature-dependent behaviors and structural evolution of poloxamer 407. *Polym. Int.* **2021**, *70*, 1282–1289.
- (70) Mortensen, K.; Batsberg, W.; Hvidt, S. Effects of PEO-PPO diblock impurities on the cubic structure of aqueous PEO-PPO-PEO pluronics micelles: fcc and bcc ordered structures in F127. *Macromolecules* **2008**, *41*, 1720–1727.
- (71) McConnell, G. A.; Gast, A. P.; Huang, J. S.; Smith, S. D. Disorder-order transitions in soft sphere polymer micelles. *Phys. Rev. Lett.* **1993**, *71*, 2102–2105.

- (72) Lodge, T. P.; Bang, J.; Park, M. J.; Char, K. Origin of the Thermoreversible fcc-bcc Transition in Block Copolymer Solutions. *Phys. Rev. Lett.* **2004**, 92, 145501.
- (73) Hamley, I. W.; Pople, J. A.; Diat, O. A thermally induced transition from a body-centered to a face-centered cubic lattice in a diblock copolymer gel. *Colloid Polym. Sci.* **1998**, *276*, 446–450.
- (74) de Lima, C. M.; Siqueira, S. M. C.; de Amorim, A. F. V.; Costa, K. B. S.; de Brito, D. H. A.; Ribeiro, M. E. N. P.; Ricardo, N. M. P. S.; Chaibunditc, C.; Yeates, S. G.; Ricardo, N. M. P. S. Effects of polypropylene glycol 400 (PPG400) on the micellization and gelation of pluronic F127. *Macromolecules* 2015, 48, 7978–7982.
- (75) Liu, T.; Chu, B. Formation of homogeneous gel-like phases by mixed triblock copolymer micelles in aqueous solution: FCC to BCC phase transition. *J. Appl. Crystallogr.* **2000**, *33*, 727–730.

### **□** Recommended by ACS

Molecular Weight-Dependent Diffusion, Biodistribution, and Clearance Behavior of Tetra-Armed Poly(ethylene glycol) Subcutaneously Injected into the Back of Mice

Shohei Ishikawa, Takamasa Sakai, et al.

APRIL 03, 2023

ACS MACRO LETTERS

READ 🗹

#### Gelation Dynamics during Photo-Cross-Linking of Polymer Nanocomposite Hydrogels

Michael C. Burroughs, Danielle J. Mai, et al.

DECEMBER 05, 2022

ACS POLYMERS AU

READ 🗹

#### Fast Healing of Covalently Cross-Linked Polymeric Hydrogels by Interfacially Ignited Fast Gelation

Yongqi Liu, Gengsheng Weng, et al.

DECEMBER 09, 2022

MACROMOLECULES

READ 🗹

#### Tuning Structure and Rheological Properties of Polyelectrolyte-Based Hydrogels through Counterion-Specific Effects

Claire Hotton, Natalie Malikova, et al.

JANUARY 20, 2023

MACROMOLECULES

READ 🗹

Get More Suggestions >